Research Article Vol. 3, No. 10 / 15 Oct 2024 / Optics Continuum 1833
OPTICS CONTINUUM

# Fully programmable holographic diffraction grating for NIR synthetic spectra generation in correlation spectroscopy

M. Chiarini,[1,*] M. Bellettato,[2] G. G. Bentini,[1,2] F. Bonafè,[2] I. Elmi,[2] V. Morandi,[2] G. Pizzochero,[2] and F. Tamarri[2]

[1] *Prometheus S.r.l., c/o CNR-IMM, Via P. Gobetti 101, 40129 Bologna (BO), Italy*
[2] *Consiglio Nazionale delle Ricerche, Istituto per la Microelettronica e i Microsistemi (CNR-IMM), Via P. Gobetti 101, 40129 Bologna (BO), Italy*
[*] *prometheus.photonics@gmail.com*

**Abstract:** Correlation spectroscopy is a powerful analytical tool for gaseous species detection, with improved sensitivity and enhanced selectivity. The application in the field of this spectroscopic technique, for remote sensing purposes, has long been prevented due to the necessity to equip the instrument with a reference 'cell' containing an actual sample of the target molecules to perform correlation measurements. A new photonic chip, based on LNOI (lithium niobate on insulator) substrates, has been developed and tested by applying MEOS (micro electro optical system) micromachining techniques. The novel photonic chip allows to dynamically generate synthetic spectra of in principle any chemical species detectable in the transparency range of LNOI (350 nm – 5500 nm wavelength). The synthetic spectrum is generated by producing a well-defined holographic phase map in the active layer of the LNOI substrate, by applying through an array of driving electrodes a calculated voltage distribution, thus rendering the photonic chip fully programmable even in real-time. The developed photonic chip is therefore able to replace the classical sample cell and can be also used to act as a reference signal modulator, as requested in a correlation spectrometer. In this work, a description of the developed technology is reported together with some preliminary results obtained in different experimental conditions.



## 1. Introduction

Correlation spectroscopy (CS) is a consolidate spectroscopic technique for gaseous species detection, providing high sensitivity and good selectivity [1,2]. The basic principles and theory of such technique are already reported in literature [3] and will not be treated in detail in this work, nevertheless, it has to be recalled that the fundamental elements allowing to implement CS measurements are to identify in, a), the presence of a reference, representative of the species to be detected and, b), a signal modulator device, frequency locked to a lock-in amplifier, allowing to properly filter and amplify the sampling signal. Here a) provides selectivity whereas b) allows to extract even very faint signals from background noise, thus ensuring high sensitivity. Also, the spectral resolution required to identify target molecules is in general relaxed with respect to the same figure as requested by conventional differential optical absorption spectroscopy (DOAS) techniques [2].

First developments of CS implied the introduction of a reference cell, physically containing a well-determined amount of the target molecule, furthermore the modulation of the reference signal was initially obtained by varying the pressure of the sample contained in the reference cell with the aid of gas pumps and properly configured hydraulic valve systems [1,2]. This approach leads to both massive and hindering apparatuses, poorly adapted to in situ applications. Furthermore, the requirement of an actual amount of the target species, physically present in the reference cell, poses non negligible limitations when e.g., hazardous, explosive, illegal etc. substances are to be

#524789 https://doi.org/10.1364/OPTCON.524789
Journal © 2024 Received 27 Mar 2024; revised 6 Sep 2024; accepted 6 Sep 2024; published 18 Sep 2024

OPTICS CONTINUUM

searched and consequently handled [4]. To circumvent all above reported problematics, different solutions have been proposed and implemented based on either ruled or holographic spectral masks, mechanically moved for reference signal modulation – e.g., either vibrating or moving on a rotation wheel - thus reducing the overall reference / reference signal modulator chain system, consequently leading to CS assemblies more adapted for on field measurement campaigns. However, such apparatuses are poorly flexible, as the static information contained in the spectral masks limits the number of molecules selectable as target species [5]. A step forward towards further miniaturization of CS systems was obtained by the introduction of MEMS (micro electro optical systems) based light modulators, allowing to implement either passive or active spectral holographic filers. In fact, following general holography principles, the spectral content of an optical beam can be recreated from the stored phase profile of a polychromatic light beam. This can be obtained, for example, by the precise surface engineering of the substrate surface, creating a suitable topology to spatially store the requested phase distribution [6,7]. A more flexible way of producing the phase profiles for spectral holography is to build a programmable diffraction grating where the individual beams of the grating can be controlled [7]. This functionality has been implemented and investigated with the introduction of optical light valves, based on mechanically adjustable micro-reflective elements (ribbons, mirrors, etc.) [8–13]. Such devices, though technologically mature and available as off-the-shelf components, present some important physical limitations, intrinsic to their electro-mechanical driving principles, and, particularly, in the switching frequencies that difficultly trespass the kHz capability.

Since about a couple of decades an alternative approach, based on electro-optical substrates, has been proposed [14,15], nevertheless, only recently these alternative solutions have been embodied in actual chips, due to the complexity of the overall architecture requested, when bulk materials are applied for their implementation [16]. In fact, to obtain efficient programmable diffractive structures on bulky electro-optical substrates a whole series of side effects shall be prevented, mainly induced by the relatively high voltages to drive the diffractive elements within a full wavelength phase shift. In fact, the drive voltages can span, as a function of the selected electrooptic material, from tens to hundreds of Volts, consequently, it is important to control the cross-talking phenomena arising from the driving structures aspect ratios, that are limited by the substrate bulky dimensions [17]. The introduction of planar technology processes on hybrid stratified substrates, LNOI, based on layers of different materials having a thickness of some tens of μm, allows to generate, applying a low driving voltage to the active layer, the electric fields required to control the refractive index via the Pockels' effect. The use of planar architecture remarkably changes the panorama as it allows to design a new family of integrated electro optic devices. In particular, using this kind of substrates, we have developed a novel miniaturized and fully programmable holographic grating, previously suggested in one of our seminal works [14], based on the embodiment of the Michelson's "echelle" grating [18] in a programmable planar technology device, opening the way to a new generation of compact and portable hyperspectral CS instruments. A description of the photonic programmable phase diffraction grating is reported in detail in the following.

## 2. Materials and methods

### *2.1. Programmable grating preparation*

The photonic programmable chips were fabricated starting from LNOI substrates procured from Nanoln, Jinan Jingzheng Electronics Co., Ltd., In particular, 10 μm thick single crystal Z-cut lithium niobate (LN) films, bonded on Si substrates were processed by means of conventional planar technology. To define the phase diffraction grating structure, periodic refractive index contrast arrays were produced in the LN active material layer by exploiting the strain induced by means of a high tensile metal film. To obtain the strain induced refractive index periodic variation, a bimetallic film was deposited on the LNOI substrates, consisting of a 100 nm Cr layer, acting as

OPTICS CONTINUUM

both adhesion and strain inducing layer, with on top a 200 nm Au layer, acting as both protecting and driving electrode layer. Both films were deposited in succession by metal evaporation within the same apparatus, i.e. without breaking the vacuum chain in between the two depositions steps, thus improving adhesion between the Au and the Cr layers. By applying conventional photolithographic techniques, Au and Cr films were patterned in periodic arrays, consisting of parallel rectangular stripes 10 to 20 mm long and 20 to 50 µm large. Arrays constituted by either 50 or 100 stripes, with 80 µm pitch were obtained by Au and Cr wet etching. The selection of these dimensions is motivated by design reasons, as reported in the following Section 3. The schematics of the geometry of the programmable phase diffraction grating (PPDG) is reported in Fig. 1(b)).

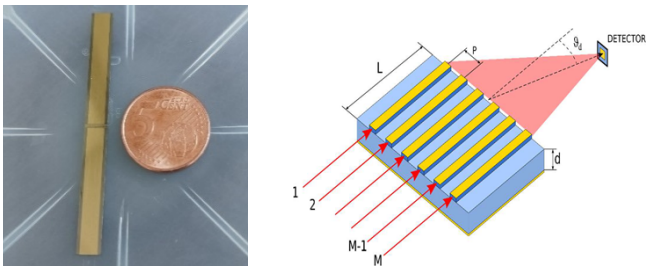


a) b)

**Fig. 1.** a) LNOI substrate with two programmable phase diffraction gratings characterized by bimetallic strain-inducing stripes, compared with a coin (21,25 mm diameter). b) Schematic of a holographic grating chip. The output far field pattern at the diffraction angle $\theta$ has the shape and the spectral content that depend on the phase shifts induced by the waveguide array. Critical design parameters are the device length, L, and thickness, d, the number M of constituting channels(waveguides), and the channels pitch, p (See Sect. 3 for details).

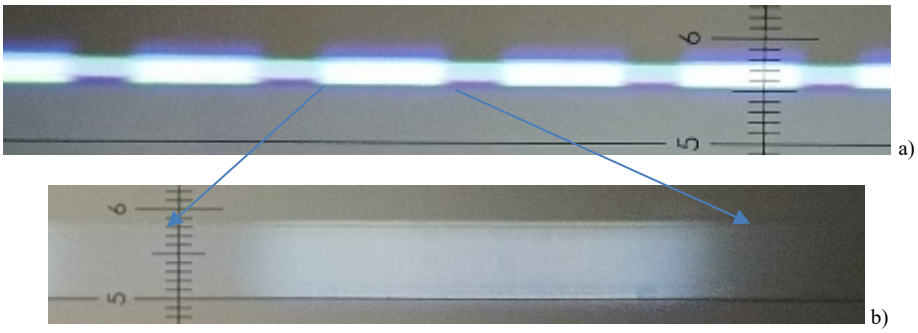


**Fig. 2.** Optical near field image of the cross-section output port at different magnifications, a) and b), showing the waveguiding effect induced by strain effect on the substrate. Scale bars are 4.8 µm and 1.1 µm for Fig. a) and b), respectively.

Finally, the substrates were dice cut to obtain single chips which were front end optically polished (see Fig. 2).

In particular, the chips were front-end optical polishing step by step verifying the quality of the diffraction figure obtained. Considering the integrated optical nature of the device, the criteria adopted to identify the end point of the polishing process concerned directly the output diffraction pattern, with particular attention to its symmetry around the central line (Figs. 3 and 4) and the insensibility of the pattern spatial distribution with respect to the light injection point [18,19].

OPTICS CONTINUUM

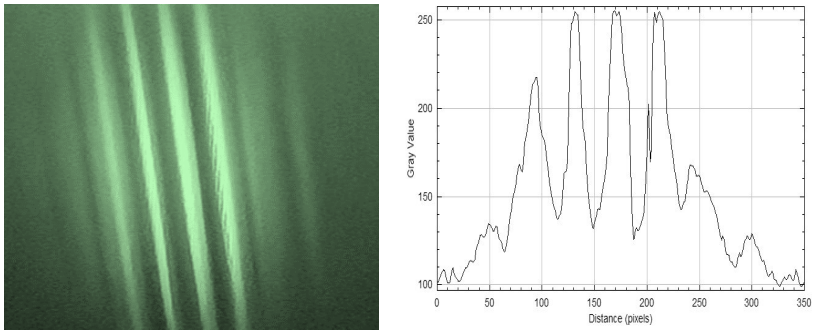


a) b)

**Fig. 3.** a) Output diffraction pattern as obtained at the end of the optical polishing with 532 nm laser, b) transverse intensity profile at the diffraction pattern peak.

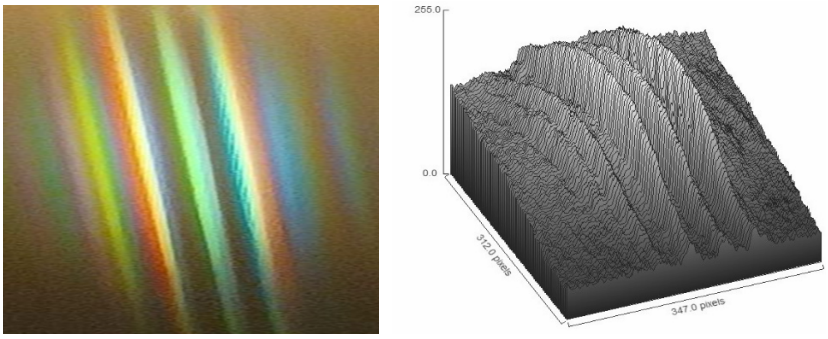


a) b)

**Fig. 4.** a) Output diffraction pattern as obtained at the end of the optical polishing with a white coherent broadband source, b) 2D intensity profile of the diffraction pattern at optical preparation process accomplishment.

### *2.2. Programmable phase diffraction grating electrical I/F*

Considering the strain induced nature of the produced PPDGs, to avoid introducing further straining elements lacking the control obtainable by planar technology, it was decided to develop a flip chip technique to directly contact the metallic stripes acting as driving electrodes in their Au layer.

Electric contact chips were fabricated based on fused silica glass substrates. A 30 nm Cr film was used as adhesion layer for a 300 nm thick Au film. By conventional photolithography followed by wet etch, the contacting structures were defined on the silica wafer. A 500 nm thick SiOx film was eventually sputtered on the substrates to insulate the metallic structures from electric contact with the PPDG driving electrodes whereas, by successive photolithographic wet etch of the upper SiOx layer, the extremity pads of the flip chip were opened and exposed. Electrogalvanic growth of copper allowed to obtain 5-micron thick contacting pads at the flip chip extremities.

Flip chips were then dice cut and properly cleaned to remove all particles resulting from cutting processes. The use of fused silica glass substrates allowed to properly align the driving electrodes of the PPDG with the ladder contacts of the ladder-like arrayed contact pads of the flip chips and then pressed in hard contact to promote electrical continuity between Cu pads and

OPTICS CONTINUUM

corresponding Au driving electrodes on PPDG. A drop of low viscosity double component epoxy resin (Epotek 301 2-FL) was poured with a micropipette at one flip chip side and eventually let it fill by capillarity the overall gap in between the PPDG and the flip chip. Once filled, the sandwich constituted by the PPDG, the epoxy resin and the flip chip were kept at 50°C for 12 h in order to promote epoxy resin polymerization and shrinkage.

It must be stressed that in this process, the shrinking of the resin due to polymerization enhances the hard contact between Cu pads and Au driving electrodes, whereas the filling of the gap with polymerized resin promotes electrical insulation between adjacent Au driving stripes on PHG.

After flip chip and PPDG integration, the hybrid chip (HC) was mounted on a dedicated PCB and wire bonded to the PCB electrical tracks for direct mounting through conventional connectors on the driving electronic board.

The electronic board has been developed starting from standard commercial components and is provided with a fast and low consumption microprocessor directly interfaced to a laptop via USB interface for its programming. The micro-processing unit drives a series of DACs modules allowing to feed up synchronously ninety-six 12 bits channels, interfaced through the PPDG PCB directly to the HC driving electrodes via the flip-chip interface, with driving voltages in the range -10 V ÷ +10 V, both dynamically and statically.

All voltage patterns, integration time, lock-in frequency, pattern sequence etc. are set by a log-in file fed to the micro-processing unit via conventional USB3 laptop I/F.

## 3. Comparison between synthetic and actual spectra

The PCB platform bearing the photonic components was connected via flats to the driving board. The HC was fed through a "white" light source, arising from a broadband NIR source (SuperK Compact Supercontinuum Laser from NTK Photonics) directly injected at the HC input side, whereas at the output, the programmed synthetic diffraction pattern was sampled at different angles by an optical fiber, coupled to a conventional NIR spectrometer (OSM2 NIR optical spectrometer from Newport), operating in the 900 nm – 1700 nm spectral window with 1.5 nm spectral sensibility.

Different target synthetic spectra were programmed, and the results obtained through direct spectroscopic measurement were compared to the expected ones, in different operating conditions (voltage pattern distribution, number of activated diffraction elements, spectral segment, etc.).

As for the detailed calculation of the voltage patterns to be applied to generate the synthetic spectrum of a selected target, the reader is addressed to Refs. [16,20–24]. Here we will only summarize the PPDG mathematical model that we used to calculate the voltage pattern, and the experimental set-up used to obtain the experimental results presented in the next chapter.

The determination of a driving voltage pattern able to introduce the required phase shifts on each waveguide for a synthetic spectra generation is the base problem for the programmability of the device. In fact, the definition of the driving voltage pattern must give rise to an electromagnetic radiation emerging form the output face of the grating that will generate the desired synthetic spectrum at a predetermined diffraction angle $\vartheta_d$.

The key point in the programming of a waveguide-based PPDG for a synthetic spectra generation is the determination of a driving voltage pattern able to introduce the required phase shifts on each of the M ridge waveguides. In this way, the electromagnetic radiation emerging form the output face of the grating will generate the desired synthetic spectrum at a predetermined diffraction angle $\vartheta_d$. In this section of the present paper, a mathematical framework for the specific case in which the functional elements are electro-optical waveguides will be derived and discussed.

Under the hypothesis of working in the Fraunhofer approximation, the diffracted field on a point of observation forming an angle $\vartheta_d$ with respect to the longitudinal axes of the system (see

OPTICS CONTINUUM

Fig. 5) can be described by the following Fourier-transform integral:

$$U(\lambda, \vartheta d) = \frac{C \cdot A}{\lambda} \int_{-\infty}^{+\infty} U'(X, \lambda) \cdot \exp(-\frac{2\pi i \sin(\vartheta d)}{\lambda}) \cdot dx, \quad (1)$$

where $C$ is a constant of proportionality, $A$ is the amplitude of the incident wave that, for sake of simplicity, is now supposed to be independent from the wavelength λ and $x$ is the spatial transverse coordinate of the PPDG output facet.

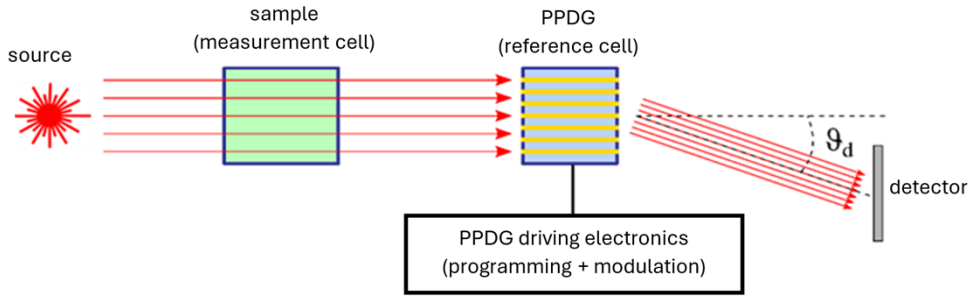


**Fig. 5.** Schematic of the set-up used in the present work showing the architecture used for correlation spectrometry experiments described in the text. In this architecture the reference cell, is substituted by the modulated programmable phase diffractive grating

In Eq. (1), *U'(x, λ)* is the near-field distribution emerging from the output facet (emitting surface) of the PMDG. For a grating with M waveguides of width W and periodicity P, this distribution can be described by the following expression:

$$U'(X, \lambda) = \sum_{m=1}^{M} \exp\left(-\gamma \cdot \frac{2\pi i L}{\lambda} \cdot \frac{Vm}{d}\right) \cdot \exp\left(-\frac{(x - mP - P/2)^2}{(\frac{W}{2})^2}\right) \quad (2)$$

where L is the electrode length, d is the device thickness, $V_m$ is the voltage applied to the m-th waveguide and γ is a constant depending both on the electro-optical characteristics and the crystallographic orientation of the substrate.

In Eq. (2), the first exponential term of the summation, describes the phase shift induced on the m-th waveguide by the local driving voltage $V_m$, whereas the second exponential term describes the mode profile emerging from each waveguide that, as a first approximation, is supposed to follow a Gaussian shape. Equation (2) clearly shows how the local phase of the field emitted by the grating and, consequently, the diffracted pattern at angle $\vartheta_d$, can be controlled through the application of a suitable set of M potentials $V_m$=1, . . . , $M$. The PPDG design and programming procedure is therefore reduced to the determination of a suitable voltage pattern, which minimizes the difference between the target spectrum of interest and the synthetic one calculated with Eqs. (1) and (2). The difference between the target and the synthetic spectra can be quantified by introducing an error function $\Delta\mathscr{E}$ of the form:

$$\Delta E = \sqrt{\sum_{1}^{N} (I_n^d - I_n)^2} \quad (3)$$

where $I_n = |U(\lambda_n)|^2$ is the intensity of the target spectrum and $I_n{}^d$ is the diffracted intensity spectrum at the considered diffraction angle $\vartheta_d$, both evaluated over the same set of $N$ wavelength within the spectral range of interest. Once this error function has been defined, the PPDG programming procedure reduces to the optimization problem of finding the minimum of $\Delta\mathscr{E}$ with respect to the control parameters ($V_1$, $V_2$, . . . $V_M$).

OPTICS CONTINUUM

In order to simplify the mathematical formalism, we can set K= (γL/d) so we can write:

$$D_m = \mathrm{K}\, V_m \tag{4}$$

thus merging in a single expression both the external driving voltage and the features of the PPDG. The new variables ($D_1$, $D_2$, ... $D_M$) have the dimension of a length, so each $D_m$ value considers the optical path differences, (at wavelength scale), among the length different waveguides. This physically is equivalent to introduce a programmable offset in the phase shift in the first term of Eq. (2). The effective voltage pattern to be applied to the different electrodes of the PPDG will then be calculated from the $D_m$ values resulting from the optimization routine once the technological parameters have been set.

To face the multivariable optimization problem, several numerical approaches have been proposed so far, among them we can cite, iterative Fourier Transform phase-retrieval algorithm, genetic algorithms, gradient-based multi-variable minimization routines [20–24].

After several tests we decided to adopt for the present investigation the Nelder-Mead simplex method [23]. This method, whose numerical implementation is available within the most common scientific computation libraries, has proven to be extremely effective for the solution of the problem described by Eqs. (1) to (3), providing a monotonic and rapid convergence toward the global minimum of the error function $\Delta\mathscr{E}$.

### 3.1. Generation of narrow band spectra

As a first test, simple narrow band synthetic spectra were generated, to verify at a very basic level the efficacy of the implemented algorithms and consequently the adherence with the theoretical background of the device. A typical result is reported in the below reported figures.

The effect of the number of waveguides (channels) on the accuracy of the synthetic spectrum reconstruction has been evaluated in the case of phase gratings having different number (10, 20, 30 and 50) of waveguides. Figures 6, 7, and 8 report the results for a single peak target.

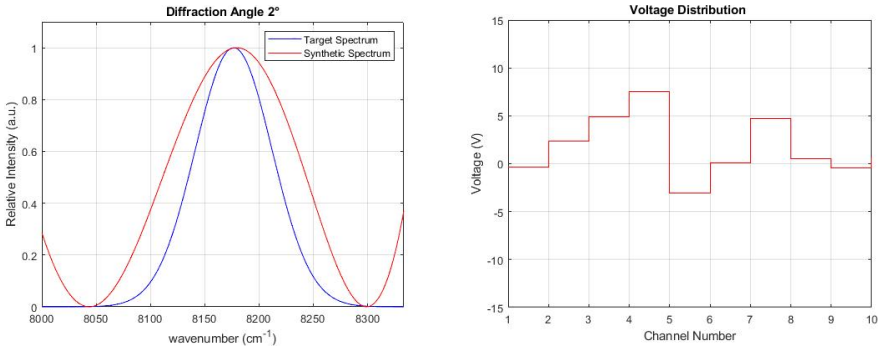


**Fig. 6.** a) simulation of single peak synthetic spectrum generation with 10 channels activated, b) calculated voltage pattern to be applied for channels drive.

From the examples of synthetic spectra reconstruction reported in Figs. 6, 7, and 8, it clearly appears that the accuracy with which can be obtained the target spectrum is dependent on the number of waveguides forming the phase grating. This involves the definition of the technological process used to fabricate it. As a rule of thumb, the higher is the number of waveguides the better is the accuracy in the reconstruction of the target spectrum. In general, this requirement involves a high number of narrow waveguides close packed.

OPTICS CONTINUUM

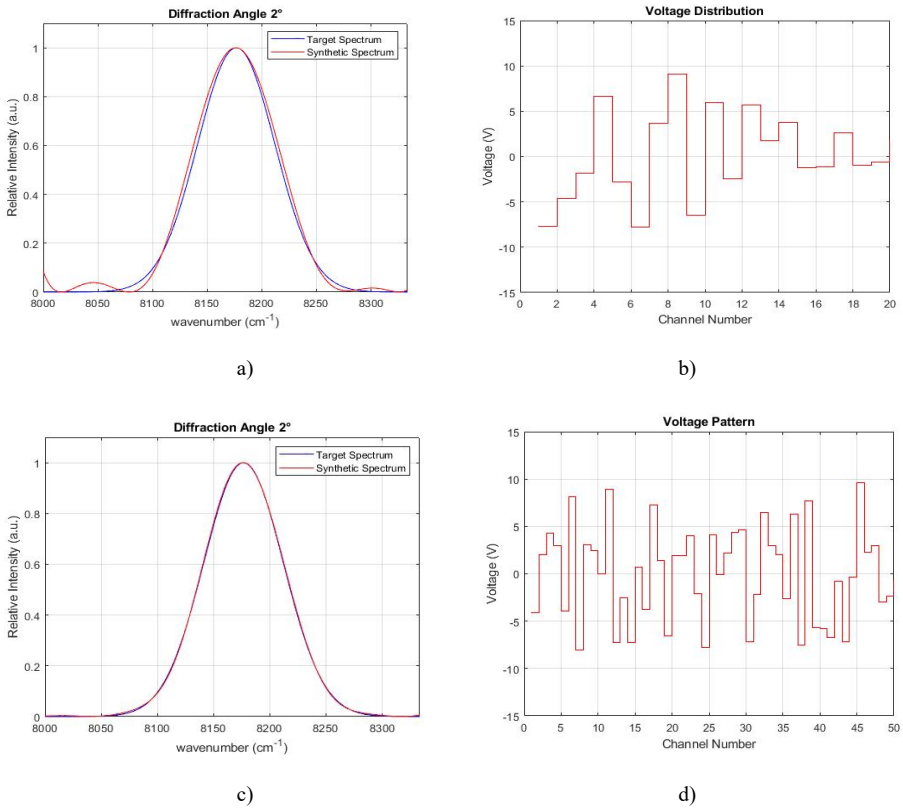


**Fig. 7.** a) simulation of single peak synthetic spectrum generation with 20 channels activated, b) corresponding calculated voltage pattern to be applied for channels drive, c) same with 50 channels and d) corresponding calculated voltage pattern.

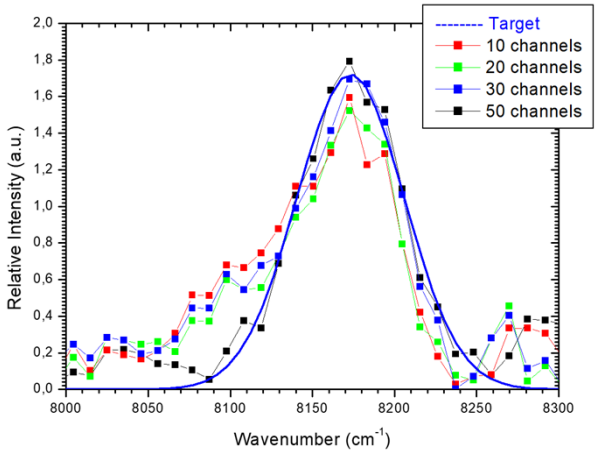


**Fig. 8.** Actual synthetic spectra obtained by application of different voltage patters, involving a progressively growing number of diffraction channels.

OPTICS CONTINUUM

One limit is that when the waveguide width is small, there is a cut-off in the upper part of the spectral window so excluding the use of the device with long wavelengths. A second limitation comes from the crosstalk that can become excessive for very close packed waveguides arrays. In conclusion it is necessary to make a trade-off between the spectral window of the synthetic spectrum and the desired accuracy of the reconstruction.

### 3.2. Generation of broad-band spectra

A successive step, fundamental for the application of the HC for CS analyses, was implemented through the generation of broad-band synthetic spectra, constituted by articulated spectral features.

An example of the effect of the PPDG programming process on an infra-red, (I.R.), region centered around the wavelength $\lambda = 1288$ nm and with a spectral window 748 nm wide is reported in Fig. 9.

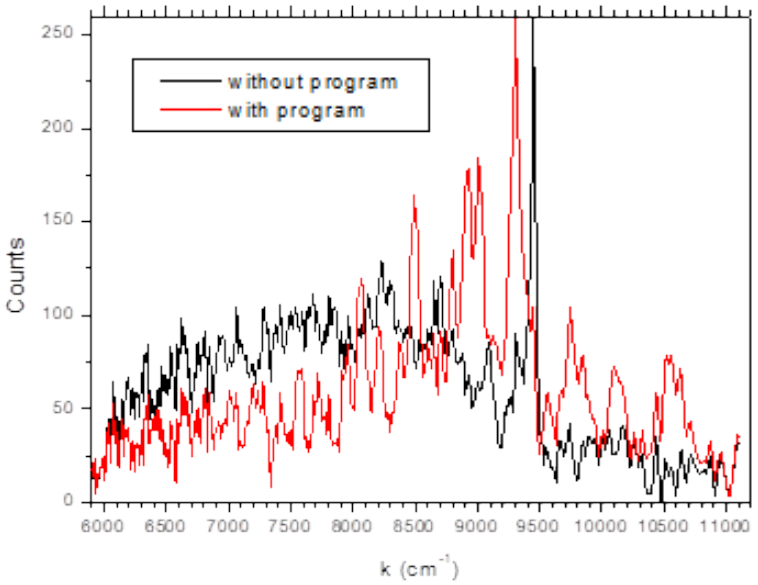


**Fig. 9.** Comparison of a rough spectrum (black line) obtained at 2° angular distance from the central diffraction order and the spectrum obtained at the same angle after the application of a calculated driving voltage program (red line), i.e. with the generation of a synthetic spectrum

Figure 9 shows the effect of the application of a programming voltage pattern on a broad band spectral window, spanning 748 nm in wavelength. In particular, the black line shows the spectral distribution registered at 2° angular distance from the central diffraction order, whereas the red line shows the spectrum obtained at the same angle, when a calculated voltage pattern is applied. From the comparison between the two spectra, it clearly appears the huge effect 'synthetically' obtained – i.e. with the application of a voltage driven phase distribution – on a very large spectral window.

With reference to the schematic architecture reported in Fig. 5, let us show the effect of the correlation process on the experimental spectrum of $CH_4$. In this case, the synthetic spectra used for the correlation process was the IR spectrum of the methane ($CH_4$), as reported in common databanks [e.g., 25]. The results, displayed in Fig. 10, give a strong indication on the accuracy of both the instrument and the synthetic spectra generation. Also, in this case, it is necessary to make a trade-off between accuracy of the reconstruction of the synthetic spectra and the architecture of the programmable phase grating, with particular reference on the number of waveguides.

OPTICS CONTINUUM

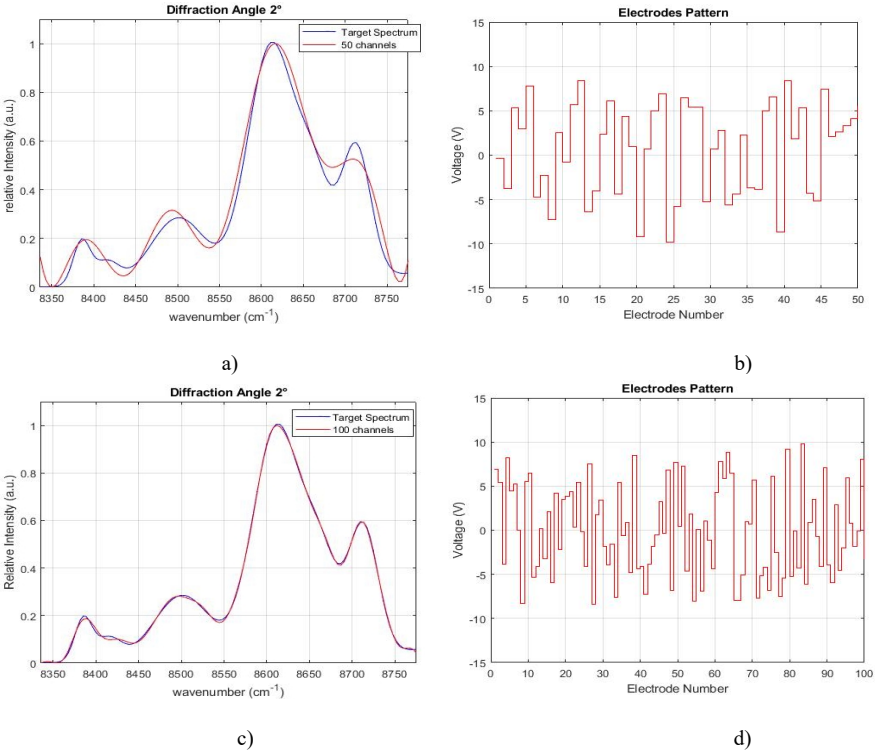


**Fig. 10.** a) Simulation of the methane spectrum as it is generated by a phase grating having an array of 50 waveguides. b) The corresponding calculated voltage pattern to be applied. c) and d) report the same for a 96-channels PPDG.

Considering that the peculiar characteristic of the Michelson's "echelle" grating is the high resolution at very small diffraction angles where the intensity is very high, it was decided to reconstruct the synthetic spectra on a wavelength window of about 50 nm in the case of two kinds of phase grating working at a fixed diffraction angle of 2° and having an array of 50 and 100 waveguides respectively. Figures 10 (a) and 10 (c) report the synthetic spectra obtained with phase gratings formed by an array of 50 and 100 waveguides respectively. Whereas Figs. 10 (b) and 10 (d) report the relative potential patterns.

In Fig. 11 the experimental analysis of the effect of the number of diffractive waveguides (channels) is reported, measuring the intensity distribution of a real spectral peak centered at 1224 nm and spectral window 70 nm wide, as a function of the number of waveguides activated in the phase grating. Also, in this case, (spectral window of 70 nm), an analysis of the efficacy of the implemented programming algorithms and the adherence of the basic theory with the actual functioning of the device was possible via the comparison of both expected, (target), and obtained results.

### *3.3. Assessment of the results*

The computer synthetized spectra and the comparison with the experimental data reported in the previous chapter demonstrate that there is a good agreement between the theoretical models developed for the functioning of the integrated programmable synthetic spectra generator and the results obtained by implementation of the programmable phase grating device fabricated by using integrated optics MEOS microfabrication techniques on LNOI substrates.

OPTICS CONTINUUM

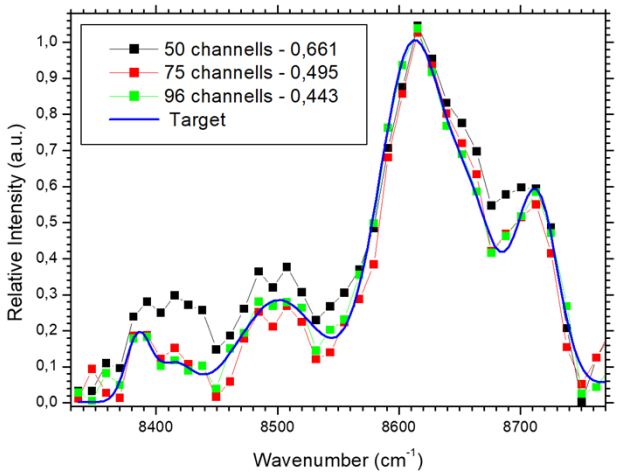


**Fig. 11.** Accuracy of the generation of synthetic spectra as a function of the activation of a progressively growing number of diffraction waveguides (channels). In the internal figure caption, the values of the parameter $\Delta\mathscr{E}$, as per Eq. (3), are reported for each activated channel set.

The main source of discrepancy observed between the generated synthetic spectra and the expected ones mainly resides on the number of diffraction channels involved, which number is in general slightly greater than the one calculated with the basic functioning model. This aspect is probably due to non-idealities introduced on actual devices during both microfabrication and principally during front-end optical preparation by means of conventional polishing techniques. This suggests that a very good control of the front-end optical surfaces is a very important parameter to control if an integrated device suitable for proper operation is required.

## 4. Conclusions

With this work we demonstrate the feasibility of fully programmable synthetic spectra generators using integrated optics MEOS microfabrication techniques on LNOI substrates. A series of HC integrated optics devices were fabricated and tested to verify the possibility of a proper application in CS instrumentation, where the integrated HC replaces the reference cells by generating programmed synthetic spectra of the analyte to be detected and measured. The tests performed on lab conditions demonstrated the capability of such device to generally generate synthetic spectra with a very good spectral correspondence with the target ones. Though it was verified that, to obtain a good correspondence between the target and the generated spectrum it is required on average a higher number of diffractive elements with respect to the number calculated ones, nevertheless with the driving of about 100 diffraction channels it is possible to properly fit spectral features < 10 nm FWHM over the whole 900 nm -1700 nm spectral window, thus indicating a spectral resolving capability, depending on the central wavelength of the synthetized spectrum, better than 1 nm at 900 nm and better than 2 nm at 1700 nm, with a nearly linear dependence with wavelength between these two extremals.

With respect to state-of-the-art holographic phase mask apparatuses, our device offers many advantages in terms of compactness and particularly flexibility. In fact, it is worth mentioning that the programmability of the device, allows to address even in real time huge numbers of target species to be detected, with a simple online reprogramming process. With respect to MEMS analogous devices, namely micromechanical optical light valves, the PPDG based on LNOI offers a great advantage in terms of switching capabilities, owing to the fact that no mechanical parts

OPTICS CONTINUUM

are involved but only electro-optical switched elements are exploited, with intrinsic switching capabilities in the realm of hundreds of MHz and more, proper of the $LiNbO_3$ based substrate.

The PPDG device, described in this work, offers the capability to synthesize in real time reference spectra of in principle any molecule detectable in the N.I.R. spectral segment with application to potentially hazardous and security problematic chemical agents, possibly present in the sampled environment atmosphere. Furthermore, the same device can be operated as reference signal modulator, thanks to the electro-optic properties of the active layer, thus implementing in a compact integrated optical solution, all the features requested in correlation spectroscopy by the reference cell, as described in the introduction. In synthesis, the above reported characteristics are compliant with the requirements of CS applications, particularly on field, where the HC can fully replace both reference cells and optomechanical succedaneums of such components. In fact, starting from the described integrated HC, a new generation of miniaturized fully programmable correlation spectrometers are under development at our labs. in particular, a first application of such miniaturized instrumentation, has been implemented in a compact correlation spectrometer, applied to perform environment analyses flying on board of an airborne drone platform, which is at present involved in on-field test campaigns, which results will be reported and described in a forthcoming paper.

**Acknowledgments.** This work was possible thanks to the Prometheus program, financed by a group of local investors, namely Mr. Aldo Artoni, Mr. Oddino Braglia, Dr. Francesca Braglia, Dr. Lorella Braglia, Mr. Sandro Braglia and Mr. Sauro Farabegoli, who promoted and granted the development of the Photonic technology described in this work. In particular, thanks to their personal effort, the described technology is nowadays patented under EU Patent EP3704544 and US Patent US11513417B2.

**Disclosures.** The authors declare no conflicts of interest.

**Data availability.** Data underlying the results presented in this paper are not publicly available at this time but may be obtained from the authors upon reasonable request.

## References

1. 1. J.P. Dakin, H.O. Edwards, and B.H. Weigl, "Progress with optical gas sensors using correlation spectroscopy," Sens. Actuators, B **29**(1-3), 87–93 (1995).
2. J.P. Dakin, M.J. Gunning, P. Chambers, *et al.*, "Detection of gases by correlation spectroscopy," Sens. Actuators, B **90**(1-3), 124–131 (2003).
3. G. S. Newcomb and M. M. Millan, "Theory, applications, and results of the long-line correlation spectrometer," IEEE Trans. On Geosci. Electr. **8**(3), 149–157 (1970).
4. M. D. Rabbett, "Filter wheel for use in a gas filter correlation system," UK Patent Appl. GB2314411A (1997).
5. Trieu-Vuong Dinh, Ji-Won Ahn, In-Young Choi, *et al.*, "Limitations of gas filter correlation: A case study on carbon monoxide non-dispersive infrared analyzer," Sens. Actuators, B **243**, 684–689 (2017).
6. M. B. Sinclair, M. A. Butler, A. J. Ricco, *et al.*, "Synthetic spectra: a tool for correlation spectroscopy," Appl. Opt. **36**(15), 3342–3348 (1997).
7. A. Ben-David, A. Ifarraguerri, and A. C. Samuels, "Correlation spectroscopy with diffractive grating synthetic spectra and orthogonal subspace projection filters," Opt. Eng. **42**(2), 325–333 (2003).
8. A. D. T. Neilson, R. Ryf, F. Pardo, *et al.*, "MEMS-based channelized dispersion compensator with flat passbands," J. Lightwave Technol. **22**(1), 101–105 (2004).
9. A. D. S. Greywall, C.-S. Pai, S.-H. Oh, *et al.*, "Monolithic fringe-field-activated crystalline silicon tilting-mirror devices," J. Microelectromech. Syst. **12**(5), 702–707 (2003).
10. M. B. Sinclair, K. B Pfeifer, M. A Butler, *et al.*, "A MEMS—Based Correlation radiometer," Proc. SPIE **5346**, 37–47 (2004).
11. M. B. Sinclair, K. B. Pfeiffer, J. B. Flemming, *et al.*, "Correlation Spectrometer," U.S. Patent 7 697 134 Bl (2010).
12. M. A. Butler, E. R. Deutsch, S. Senturia, *et al.*, "A MEMS-based programmable diffraction grating for optical holography in the spectral domain," *International Electron Devices Meeting*. Technical Digest, (Cat. No.01CH37224), 41.1.1-41.1.4, Washington, DC, USA, (2001).
13. G. B. Hocker, D. Youngner, M. A. Butler, *et al.*, "The polychromator: a programmable MEMS diffraction grating for synthetic spectra," *Solid-State Sensor and Actuator Workshop, Hilton Head Island, SC (US)*, (2000).
14. G. G. Bentini, A. Parini, M. Chiarini, *et al.*, "Monolithic fully integrated programmable microdiffraction grating based on electro-optical materials," Proc. SPIE **6593**, 659325 (2007).
15. M. Mony, E. Bisaillon, E. Shoukry, *et al.*, "Reprogrammable optical phase array," Appl. Opt. **46**(18), 3724–3729 (2007).
16. A. Parini, M. Chiarini, G. Basti, *et al.*, "Lithium niobate-based programmable micro-diffraction device for wavelength-selective switching applications," Proc. SPIE **11163**, 111630C (2019).

OPTICS CONTINUUM

17. P. De Nicola, S. Sugliani, G. B. Montanari, *et al.*, "Fabrication of smooth ridge optical waveguides in LiNbO3 by ion implantation-assisted wet etching," J. Lightwave Technol. **31**(9), 1482–1487 (2013).
18. A. Michelson, "Recent advances in spectroscopy," Nobel Lecture December 12 (1907).
19. C. Yang and X. Chen, "Effect of grating ruling machine system errors on grating spectral performance," Appl. Sci. **12**(19), 10174 (2022).
20. G. Zhou, F. E. H. Tay, and F. Chau, "Design of the diffractive optical elements for synthetic spectra," Opt. Express **11**(12), 1392–1399 (2003).
21. H. E. Kondakci and A. F. Abouraddy, "Diffraction-free space–time light sheets," Nat. Photonics **11**(11), 733–740 (2017).
22. S. Taravati and G. V. Eleftheriades, "Generalized space-time-periodic diffraction gratings: theory and applications," Phys. Rev. Appl. **12**(2), 024026 (2019).
23. J. A. Nelder and R. Mead, "A Simplex method for function minimization," The Computer Journal **7**(4), 308–313 (1965).
24. J. R. Fienup, "Phase retrieval algorithms: a comparison," Appl. Opt. **21**(15), 2758–2769 (1982).
25. , "HiTran Database," HiTran, 1982, https://hitran.org.